Available online at www.sciencedirect.com
SCIENCE DIRECT
Cement and Concrete Research 36 (2006) 1354–1361
Cement and Concrete Research

Modelling of steel fiber-reinforced concrete under multi-axial loads

Somsak Swaddiwudhipong *, Puay Eng Constance Seow

Department of Civil Engineering, National University of Singapore, 10, Kent Ridge Crescent, 119260 Singapore, Singapore

Received 5 August 2005; accepted 16 March 2006

Abstract

Fifty-four plain concrete and steel fiber-reinforced concrete (SFRC) plate specimens containing 0.5%, 1.0% and 1.5% of hooked fibers were tested under biaxial compression. The experimental results obtained were used to verify a failure surface developed earlier by the authors for SFRC under multi-axial loads. An equation has also been proposed in this study to predict the strain at failure for SFRC under multi-axial loads, ε_{ci}. The proposed failure criterion and equation to predict ε_{ci} were incorporated into a constitutive model in a well-established finite-element software, ABAQUS. Experiments of SFRC plate specimens under multi-axial loads and beams under two-point load were modeled to illustrate the application of the failure surface to SFRC under varying load conditions. Good agreement between analytical and experimental results is observed.

Keywords: Failure surface; Compressive strength; Finite-element analysis; Fiber reinforcement; Modeling

1. Introduction

When plain concrete is subjected to tension, the initiation and growth of inherent micro-cracks reduces the load-carrying area and increases the stress concentration at critical crack tips, causing the cracks to propagate further. Failure of the concrete occurs if these cracks are not effectively arrested [1]. The presence of fibers in steel fiber-reinforced concrete (SFRC), however, helps to restrain early crack growth and transfer load to the uncracked parts of the concrete matrix, thus enhancing its durability and enabling an otherwise brittle material to withstand higher tensile loads at failure. SFRC also has a greater resistance to impact, fatigue and repeated dynamic loading [2,3], making it a suitable material for constructing dams, airport runways and walls of nuclear reactor plants. These structures are normally subjected to multi-axial states of stress and thus necessitate the use of finite-element analysis and an appropriate constitutive model to simulate their behavior. Knowledge of the stress and strain at failure (R_{ci} and ε_{ci}) is required, among other parameters, to accurately define the shape of the stress–strain curve of concrete under uniaxial or multi-axial loads [4–6].

While the behavior of plain concrete under multi-axial loads has been studied and well-documented by many researchers [6–8], experiments on SFRC under multi-axial loads and models to predict the stresses and strains at failure under these load conditions have been relatively few. Nielsen [9] proposed a bi-linear failure criterion for high-strength steel fiber-reinforced mortar under axi-symmetrical loads, while Hu et al. [10] developed a biaxial failure curve which may be modified to fit the different failure envelopes of SFRC containing varying amounts and types of fiber. This was achieved by calibrating the biaxial failure curve to suit each specific mix of SFRC using experimental data points of SFRC failing under four different biaxial load combinations, uniaxial compression and uniaxial tension.

However, due to the constraints in testing equipment and limited publications on SFRC under multi-axial loads, the required experimental data may not be readily available for the specific type of SFRC being studied, as highlighted by Padmarajaiah and Ramaswamy [11]. In addition, the aforementioned failure criteria are only applicable to the specific load cases of axi-symmetrical or biaxial loads. In view of this, Seow and Swaddiwudhipong [12] proposed a unified failure surface which is suitable for use with

* Corresponding author. Tel.: +65 6874 2173; fax: +65 6779 1635.
E-mail address: cvesomsa@nus.edu.sg (S. Swaddiwudhipong).

0008-8846/$ - see front matter © 2006 Elsevier Ltd. All rights reserved.
doi:10.1016/j.cemconres.2006.03.008

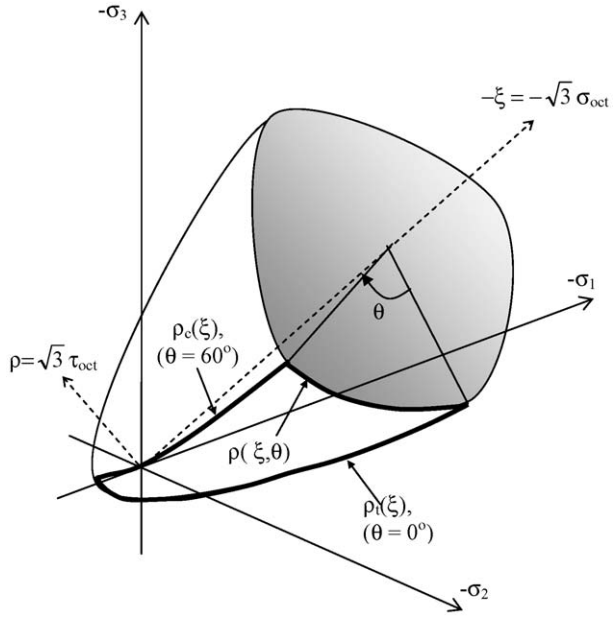

Fig. 1. Failure surface in the Haigh–Westerguard stress space.

normal, high-strength and steel fiber-reinforced concrete under any multi-axial load combination. A systematic method has also been developed for adjusting the failure surface to account for different types and volume fractions of steel fiber, using only two experimentally determined parameters: the uniaxial compressive strength, f_{cu}, and the ultimate bond strength of the fiber, τ_u. In order to verify this proposed failure surface, biaxial experiments on SFRC plates containing hooked fibers were conducted in this study. An expression to predict the strains at failure for SFRC under multi-axial loads, ε_{ci}, has also been proposed. The proposed failure surface and equation to predict ε_{ci} were incorporated into a constitutive model and used in a finite-element software to model the plate specimens tested in this study and SFRC beams tested by Lim [13]. The analytical and experimental results showed good agreement, thus validating the proposed criteria for predicting the stresses and strains at failure in SFRC under multi-axial loads.

Table 1
Properties of concrete

Mix	Test	Age (days)	Average value (MPa)
NC	Cube strength, f_{cu}	28	31.06
	Splitting tensile strength, f_t	28	3.01
	Young's modulus, E_o	28	20.04×10^3
	Uniaxial plate strength, f_c	35–45	22.96
SC-0.5	Cube strength, f_{cu}	28	32.94
	Splitting tensile strength, f_t	28	4.13
	Young's modulus, E_o	28	18.75×10^3
	Uniaxial plate strength, f_c	35–45	22.89
SC-1.0	Cube strength, f_{cu}	28	28.27
	Splitting tensile strength, f_t	28	3.31
	Young's modulus, E_o	28	18.49×10^3
	Uniaxial plate strength, f_c	35–45	21.77
SC-1.5	Cube strength, f_{cu}	28	33.31
	Splitting tensile strength, f_t	28	4.33
	Young's modulus, E_o	28	20.94×10^3
	Uniaxial plate strength, f_c	35–45	23.07

2. Proposed failure surface for SFRC

The five-parameter failure surface is illustrated in Fig. 1. It is described in the three-dimensional Haigh–Westergaard stress space by quadratic tensile and compressive meridians, ρ_t and ρ_c, when the angle of similarity, θ, is 0° and 60°, respectively, and an elliptical curve, $\rho(\xi,\theta)$, to interpolate between ρ_t and ρ_c. Due to a six-fold symmetry, the following three equations are sufficient to define the entire failure surface [12]:

$$\frac{\xi}{f_{cu}} = a_2\left(\frac{k\rho_t}{f_{cu}}\right)^2 + a_1\left(\frac{k\rho_t}{f_{cu}}\right) + a_0 \tag{1}$$

$$\frac{\xi}{f_{cu}} = b_2\left(\frac{\rho_c}{f_{cu}}\right)^2 + b_1\left(\frac{\rho_c}{f_{cu}}\right) + b_0 \tag{2}$$

$$\rho(\xi,\theta) = \frac{2\rho_c(\rho_c^2-\rho_t^2)\cos\theta + \rho_c(2\rho_t-\rho_c)[4(\rho_c^2-\rho_t^2)\cos^2\theta + 5\rho_t^2-4\rho_t\rho_c]^{1/2}}{4(\rho_c^2-\rho_t^2)\cos^2\theta + (\rho_c-2\rho_t)^2} \tag{3}$$

where

$$a_0 = b_0 = 0.1732,$$

$$a_2 = -0.1597, a_1 = -1.455$$

$$b_2 = -0.1746, b_1 = -0.778 \tag{4}$$

and

$$\cos\theta = \left[\frac{3(\sigma_3-\sigma_m)}{\sqrt{6}\sqrt{\sigma_1^2+\sigma_2^2+\sigma_3^2-3\sigma_m^2}}\right] \quad \text{For } \sigma_3\geq\sigma_2\geq\sigma_1 \tag{5}$$

f_{cu} is the uniaxial compressive strength of concrete, $\xi=\sqrt{3}\,\sigma_{oct}$ and $\rho=\sqrt{3}\,\tau_{oct}$, where σ_{oct} and τ_{oct} are the octahedral normal and shear stress, respectively. σ_i (i=1–3) is the principal normal stress in the ith direction and σ_m is the mean stress.

Since fibers help to bridge tensile cracks in concrete, a coefficient k was introduced in Eq. (1) to account for the

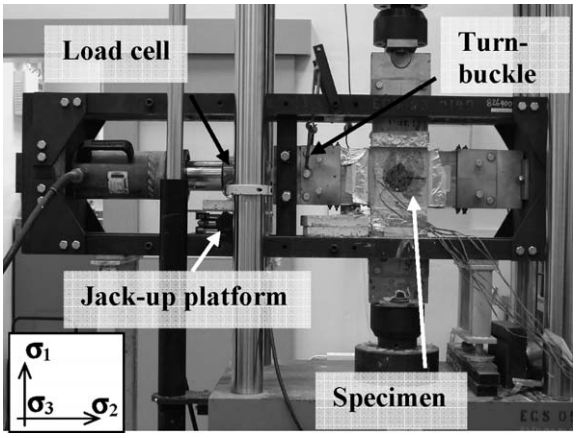

Fig. 2. Experimental set-up for biaxial tests.

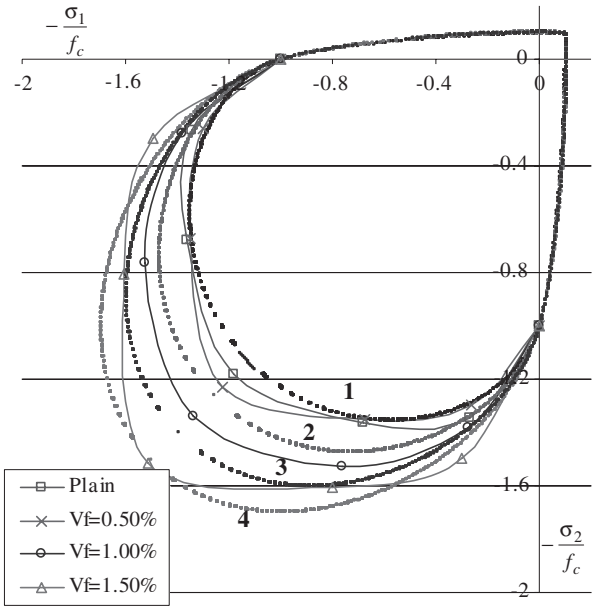

Fig. 3. Experimental and predicted biaxial curves.

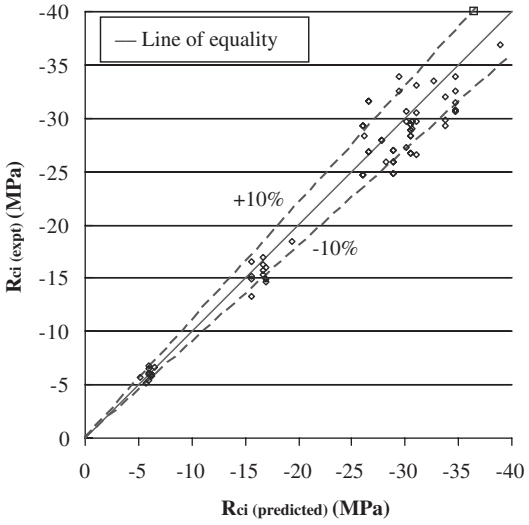

Fig. 4. Experimental and predicted stress at failure.

increase in the observed stress at failure along ρ_t, due to the confining effect of different amount and types of fibers. As the failure surface is determined by interpolating between ρ_t and ρ_c, an increase in ρ_t will also result in a change in the shape of the failure surface, thus accounting for the effect of fiber in SFRC subjected to other load ratios. The value of k is equal to 1 in plain concrete and may be determined by Eq. (6) for SFRC:

$$k = \frac{-a_1 - \sqrt{a_1^2 - 4a_2\left[a_0 + \frac{2}{\sqrt{3}}\left(\frac{f_{cc}}{f_{cu}}\right)\right]}}{a_2\sqrt{\frac{8}{3}}\left(\frac{f_{cc}}{f_{cu}}\right)} \quad (6)$$

where the coefficients a_0, a_1, a_2, are given in Eq. (4) and f_{cc} is the stress at failure for concrete subjected to 1:1 biaxial compression. Further details of the failure surface and a method to predict f_{cc} in the absence of suitable experimental data have been presented in reference [12].

3. Experimental program

3.1. Preparation and testing of specimens

Plate specimens were prepared for biaxial testing using a plain concrete mix and three SFRC mixes containing 0.5%, 1.0% and 1.5% of hooked steel fibers (Mixes NC, SC-0.5, SC-1.0 and SC-1.5, respectively). Pre-blended cement containing 65% granulated blast furnace slag and 35% ordinary Portland cement was used in this study and the mix proportion of cement, water, sand and crushed granite per cubic meter of the plain concrete mix is 361.7 kg, 242.5 kg, 829.8 kg and 867.5 kg, respectively. For SFRC mixes, the percentage of plain concrete cast per unit volume was adjusted to account for the different volume fractions (V_f) of steel fibers added. For example, Mix SC-1.5 consisted of 1.5% of steel fibers and 98.5% of plain concrete per unit volume. Given the small dimensions of the test specimens, only crushed gravel aggregates passing through a 9.5-mm sieve were used, in accordance with BS 8110-1 (1997) [14]. Hooked fibers of 30 mm length and 0.55 mm diameter, with the trade name Dramix, were selected for the SFRC mixes as they provide better anchorage than straight fibers. These fibers have a minimum tensile strength of 1100 MPa and density of 7850 kg/m^3.

The material properties for each mix were determined as follows: the uniaxial cube strength, f_{cu}, was obtained from testing 100-mm cubes, splitting tensile strength, f_c', and Young's modulus, E_o, from testing cylinders of diameter 100 mm and height 200 mm, and uniaxial plate strength, f_c, from testing 150×150×40-mm plate specimens. The averaged results from three specimens per test are presented in Table 1. All specimens required for the aforementioned tests were cast on the same day for each mix and covered with a plastic sheet to prevent moisture loss. They were demoulded after 1 day and cured in the fog room at a relative humidity of 95% and temperature of 27±2 °C till the age of 7 days. Thereafter, they were air cured at 28±2 °C. To achieve a uniform distribution of fibers and avoid end effects in the plate specimens, the 150×150×40-mm

Table 2
Values used to rotate $\rho_{t(SFRC)}$

Proposed biaxial curve	Experimental mix	Volume fraction, V_f (%)	k	Experimental f_{cc} (MPa)	Predicted f_{cc} (MPa)	Experimental f_{cc}/predicted f_{cc}
1	NC	0.0	1.000	27.09	26.04	1.040
2	SC-0.5	0.5	0.980	28.15	28.92	0.974
3	SC-1.0	1.0	0.962	29.17	30.52	0.956
4	SC-1.5	1.5	0.949	34.90	34.74	1.005

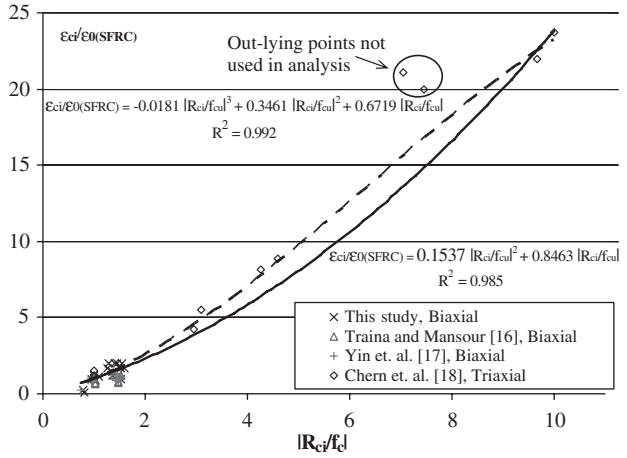

Fig. 5. Proposed equation to predict ε_{ci}.

specimens were obtained from the middle section of 150-mm cubes that were sliced using a masonry saw at the age of 21 days. They were then tested between the ages of 35 and 45 days using a biaxial testing set-up shown in Fig. 2. The Instron machine applied a monotonically increasing vertical load at a rate of 0.2 mm/min while the horizontal load was supplied simultaneously using the hydraulic jack, according to the required load ratio. Brush platens were used to transfer the loads to the specimens as they help to minimize the friction between the platen and specimen, thus reducing undesirable shear stresses in the specimen. As it is not possible to cast specimens with sides that are perfectly perpendicular, the top and left platens were connected to rockers which can accommodate up to 4.5° rotations in the loading plane. A 45° strain rosette attached to each of the unloaded surface of the specimen was used to monitor the states of strain during the tests. Further details concerning the experimental design and procedure have been elaborated by Seow [15].

3.2. Stress at failure

A minimum of three plate specimens was tested for each of the four compressive load ratios, namely, 1:0, 1:0.2, 1:0.5 and 1:1. Additional specimens were also tested to confirm any unusual results. It was observed that specimens with large discrepancies in the strain readings of both the unloaded faces failed prematurely at a lower strength, suggesting that this group of specimens was subjected to bending due to minute out-of-plane rotations of the platens during loading. As these experimental results were not reflective of the actual strength at failure, they were not included in the determination of the experimental trend in the biaxial failure curves shown in Fig. 3, which was obtained through averaging the results of two specimens per load case in each mix. The point of Mix SC-1.5 failing under 1:1 biaxial compression is an exception, where the result of only one specimen was used as the rest of the specimens had shown a poor correlation between the front and back strain readings and failed prematurely. The theoretical biaxial failure curves degenerated from the failure surface proposed by Seow and Swaddiwudhipong [12] marked 1–4 are also presented in

Table 3
Details of the finite-element models for SFRC specimens

Specimens	Material properties				Mesh size (mm)	Number of increments
	f_{cu} (MPa)	f_t (MPa)	E (GPa)	v		
Fig. 6	28.27	3.31	18.5	0.18	37.5	100
SFRC beam	34	3.4	28.0	0.2	30	36

Fig. 3. The mix designation corresponding to each curve label, the values of k and the predicted values of f_{cc} used in the formulation of the failure surfaces for SFRC are summarized in Table 2. It can be observed from Table 2 and Fig. 3 that as the volume fraction of fiber increases, so does the predicted value of the equal biaxial compressive strength of SFRC, f_{cc}. This results in an elongated biaxial failure envelope which is consistent with the experimentally observed trend. The predicted values of f_{cc} agree reasonably well with the experimental results. The shapes of the theoretical biaxial failure curves also approximate closely those observed in the experiments. It should, however, be noted that the experimental results for Mix SC-0.5 do not show a significant improvement in the strength of SFRC over plain concrete. This may be due to the small amount of fibers added to the mix and the truncation of some of these in the process of slicing the 150-mm cubes to obtain the plate specimens. While the truncation of some fibers also occurred in the preparation of specimens from the other mixes, the amount of fibers used in Mixes SC-1.0 and SC-1.5 was sufficient for the beneficial effects of the remaining whole fibers to be observed. In contrast, the small amount of fibers used in Mix SC-0.5 resulted in a smaller number of whole fibers remaining in the specimen after slicing. It may also be possible that the fibers were not evenly dispersed during the casting of the concrete. The aforementioned two factors could thus have made the strength improvement of Mix SC-0.5 less apparent when compared with the strength of the plain concrete specimens. In spite of this, the predictions of the failure surface are mostly within ±10% of all

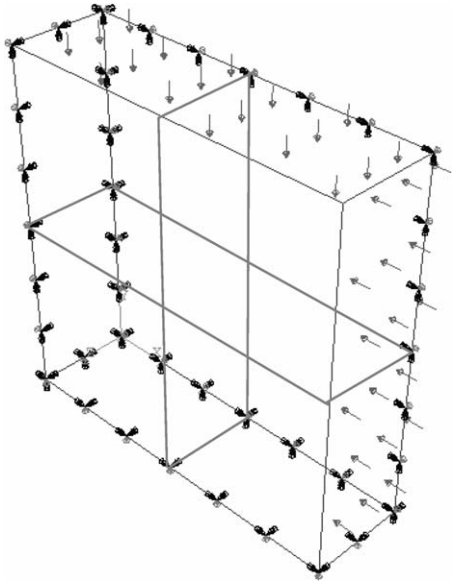

Fig. 6. Finite-element model of a plate under biaxial loads.

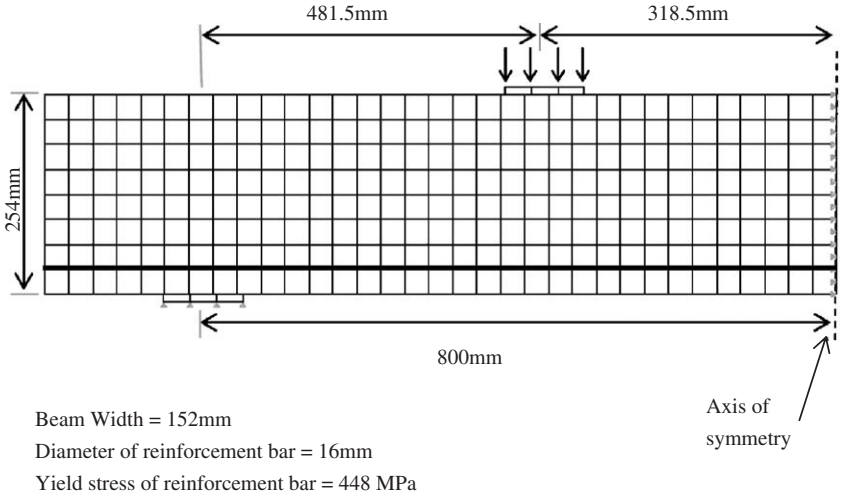

Fig. 7. Finite-element model for SFRC beams.

the experimental data, as illustrated in Fig. 4, and the mean value of ($R_{ci(expt)}/R_{ci\ (predicted)}$) for all the biaxial data points is 0.963 while the standard deviation is 0.0744.

3.3. Strain at failure

A study of the experimental stress–strain curves suggested that the compressive strain at failure in a particular direction for SFRC under multi-axial loads, $\varepsilon_{ci(SFRC)}$, was influenced significantly by the load applied and the stress at failure, R_{ci}, in that direction. When the value of R_{ci} was greater than f_{cu}, so was the value of $\varepsilon_{ci(SFRC)}$ as compared to that of the strain at failure in SFRC under uniaxial compression, $\varepsilon_{0(SFRC)}$. The reverse was also true when R_{ci} was less than f_{cu}. The same trends were observed by other researchers for plain concrete under multi-axial loads. Darwin and Pecknold [7] proposed the following equation relating $\varepsilon_{ci(NC)}$ to $\varepsilon_{0(NC)}$ and $|R_{ci}/f_{cu}|$:

$$\varepsilon_{ci(NC)} = |\varepsilon_{0(NC)}|\left[1.6\left|\frac{R_{ci}}{f_{cu}}\right|^3 - 2.25\left|\frac{R_{ci}}{f_{cu}}\right|^2 - 0.35\left|\frac{R_{ci}}{f_{cu}}\right|\right] \quad (7)$$

where $\varepsilon_{0(NC)}$ is the uniaxial compressive strain at failure in plain concrete. This equation developed for plain concrete normally over-predicts the values of $\varepsilon_{ci(SFRC)}$ and, hence, should be altered before adopting it for implementation with SFRC. It is postulated that the expression for determining $\varepsilon_{ci(SFRC)}$ takes on a similar polynomial form as Eq. (7), with a new set of coefficients obtained from regression analysis of additional experimental data. The strain readings averaged from the rosettes on both unloaded surfaces of the specimens were used to calculate the principal strains at failure presented in Fig. 5. To alleviate the undesirable effect of eccentric loadings which were apparent in the testing of certain specimens, only the results from 16 plate specimens with well correlated readings from both sets of strain rosettes in each test were included in the analysis. These data points were further supplemented by the values of $\varepsilon_{ci(SFRC)}$ for SFRC under biaxial and triaxial loads obtained by Traina and Mansour [16], Yin et. al. [17] and Chern et. al. [18]. These values were collated and presented in the same figure.

Similar to the equation proposed for plain concrete, it is suggested that either a continuous quadratic or cubic curve is sufficient to predict $\varepsilon_{ci(SFRC)}$ for the whole range of $|R_{ci}/f_{cu}|$. By imposing the condition that the sum of the coefficients of $|R_{ci}/f_{cu}|=1.0$, it was ensured that the equation will degenerate back to the uniaxial case when $R_{ci}=f_{cu}$ and $\varepsilon_{ci(SFRC)}=\varepsilon_{0(SFRC)}$. A

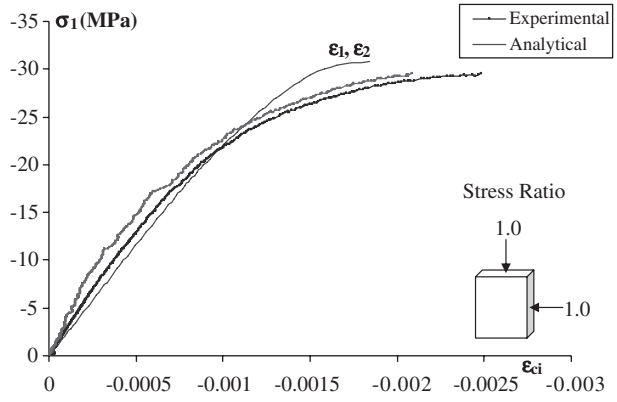

Fig. 8. SFRC plate with hooked fibres under 1:1 compression.

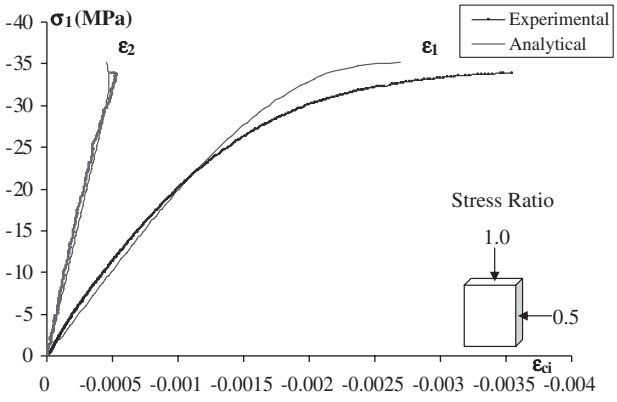

Fig. 9. SFRC plate with hooked fibres under 1:0.5 compression.

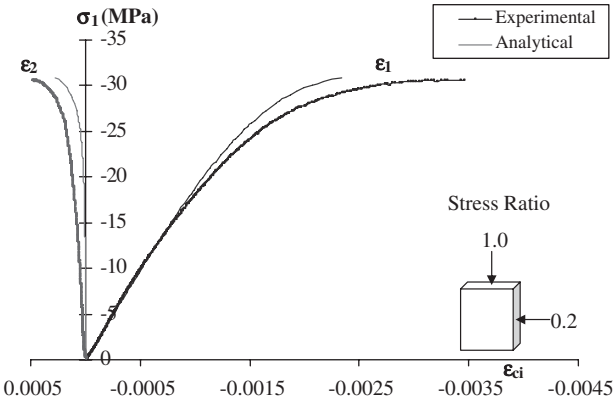

Fig. 10. SFRC plate with hooked fibres under 1:0.2 compression.

statistical analysis using the method of least-squares estimation was then carried out to determine suitable coefficients for the polynomials. For a cubic and quadratic expression, respectively, Eqs. (8) and (9) were found to give the best fit to the experimental data shown in Fig. 5.

$$\varepsilon_{ci(SRFC)} = |\varepsilon_{0(SFRC)}|\left[-0.0181\left|\frac{R_{ci}}{f_{cu}}\right|^3 + 0.346\left|\frac{R_{ci}}{f_{cu}}\right|^2 + 0.672\left|\frac{R_{ci}}{f_{cu}}\right|\right] \quad (8)$$

$$\varepsilon_{ci(SRFC)} = |\varepsilon_{0(SFRC)}|\left[0.154\left|\frac{R_{ci}}{f_{cu}}\right|^2 + 0.846\left|\frac{R_{ci}}{f_{cu}}\right|\right] \quad (9)$$

Although Eq. (8) gives a closer fit to the entire range of experimental data, it was observed that Eq. (9) had a lower sum of least squares and provided a better prediction of $\varepsilon_{ci(SFRC)}$ when $|R_{ci}/f_{cu}|$ is less than 2, where most of the experimental data is clustered. Finite-element analyses using both equations carried out by Seow [15] on the experiments conducted by Traina and Mansour [16] concur that Eq. (9) gives a better estimate of $\varepsilon_{ci(SFRC)}$ for concrete under uniaxial and biaxial load. As the values of $|R_{ci}/f_{cu}|$ encountered in engineering problems typically range between 0 and 2, Eq. (9) was adopted in the constitutive model for finite-element analyses reported in this study. More experimental data of the strains at failure in concrete subjected to triaxial loads are required to conclusively determine which equation is more suitable for use with the full range of $|R_{ci}/f_{cu}|$.

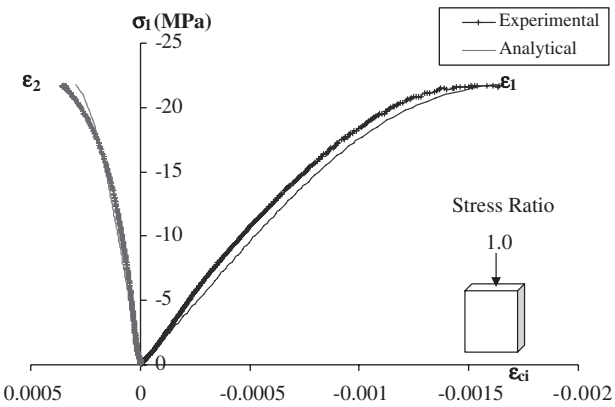

Fig. 11. SFRC plate with hooked fibres under uniaxial compression.

Table 4
Comparison of ultimate stress for plates tested in this study

Load case	Ultimate stress at failure, R_{c1} (MPa)		% difference
	Experimental	Predicted	
1:1	−29.5	−30.75	4.33
1:0.5	−33.9	−35.19	3.93
1:0.2	−30.6	−30.80	0.60
1:0	−21.7	−21.75	0.32

4. Finite-element analysis

4.1. Finite-element models

The failure surface proposed by Seow and Swaddiwudhipong [12] and the equation for predicting ε_{ci} were incorporated into a constitutive model for SFRC [19] and implemented via a user subroutine in a well-established finite-element software, ABAQUS. SFRC plate specimens under various load combinations and beams under two-point loads were then modeled to verify the accuracy of the proposed equations. The material properties, mesh size and number of increments used in the modeling of each experiment are summarized in Table 3. As quadratic elements perform more efficiently than linear elements, they were employed in all the analyses in the present study. 20-noded, solid elements were used in the three-dimensional analysis of the biaxial testing of plate specimens, while 8-noded plane stress elements were used to model the beams in a two-dimensional, plane stress analysis. The steel reinforcement bars in the beams were modeled using 3-noded truss elements.

Due to symmetry in the *x*-, *y*- and *z*-planes of the plate specimens, only one-eighth of the specimen was considered. Since displacement perpendicular to the planes of symmetry is

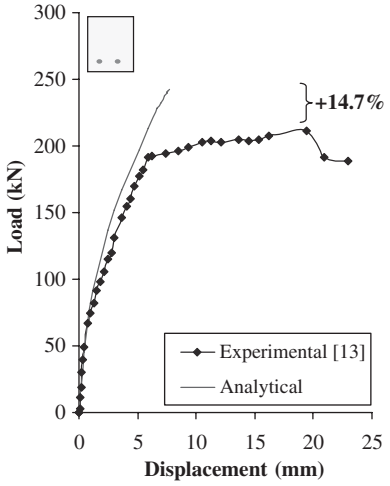

Fig. 12. Experimental and finite-element load–displacement curves for beam 2/0.5.

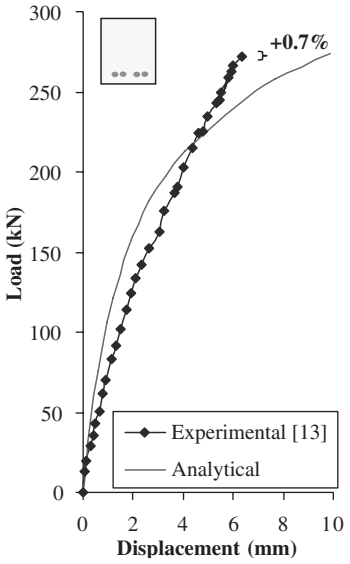

Fig. 13. Experimental and finite-element load–displacement curves for beam 4/0.5.

not allowed, roller supports were imposed at all the nodes on the planes of symmetry. The compressive loads are then applied as illustrated in Fig. 6. In the actual experiments on the SFRC beams, loads and reactions were applied through semicircular rollers and steel load platens. As these beams have geometric and load symmetry about the vertical axis at the center of the beam, only the left half of the beam was considered in the analysis and symmetrical conditions were imposed on the plane of symmetry, as shown in Fig. 7. Interface elements were also modeled between the steel platens and the beam elements to allow for separation of the beam and platen surfaces during loading.

4.2. Results of plate specimens under biaxial loads

A series of plate specimens from Mix SC-1.0 was modeled for the biaxial load ratios of 1:1, 1:0.5, 1:0.2 and uniaxial compression. The stress–strain curves for the aforementioned load cases are displayed in Figs. 8–11, respectively. For concrete under 1:1 biaxial compression, the strains monitored on the unloaded surfaces should be identical as equal loads are applied on the other four remaining faces. This is reflected in the analytical stress–strain curve in Fig. 8; however, a slight deviation of compressive strains is observed in the experimental curves. This may be due to the non-homogeneity of the concrete matrix or the difficulty in ensuring that the loads applied to the specimen were exactly equal. In spite of this, a good agreement is observed between all the analytical and experimental stress–strain curves.

The experimental and predicted values of stress at failure of the specimens in the direction under greatest compressive load, R_{c1}, are summarized in Table 4. The stress at failure in the other direction, R_{c2}, is proportional to R_{c1} and may be calculated from the load ratio which the specimens were subjected to. The predicted values of stress at failure for all the experiments modeled are within 5% of the experimental data. The good agreement between the finite-element and experimental results presented in this study demonstrates the potential of the proposed failure surface and the equation to predict ε_{ci} to give accurate predictions of the behavior of SFRC when they are incorporated into a constitutive model.

4.3. Results of beams under two-point load

Two SFRC beams containing a volume fraction of 0.5% of hooked fibers tested by Lim [13] were analyzed. The beams 2/0.5 and 4/0.5 contain two and four reinforcement bars, respectively,

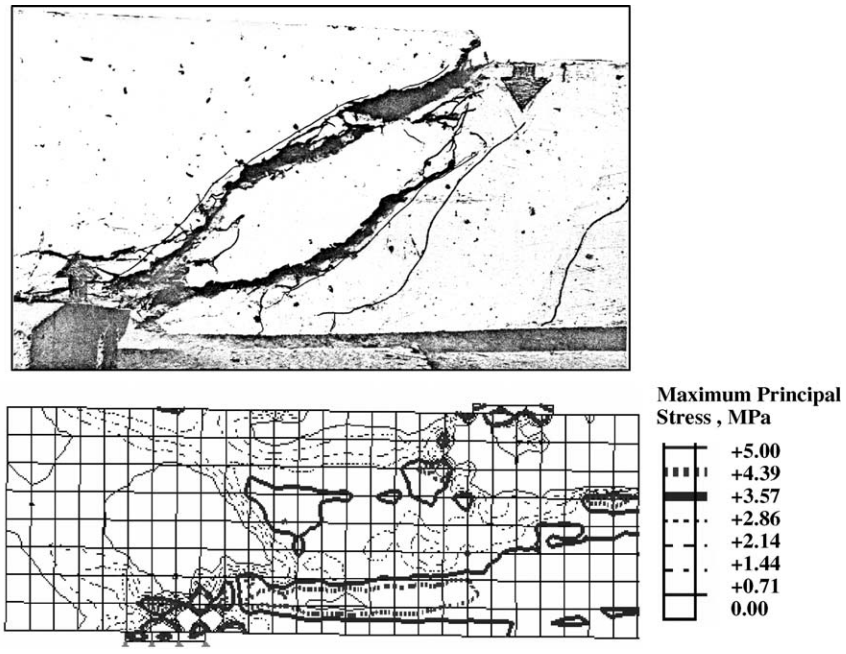

Fig. 14. Shear failure and stress contour of beam 4/0.5.

and their analytical and experimental load–displacement curves are depicted in Figs. 12 and 13. It is observed that the experimental load–displacement curves are softer than the analytical results. This is expected as displacement-based finite-element analysis is known to provide a stiffer model than the actual behavior of the structure. It is also apparent that the analytical model is stiffer for beam 2/0.5 compared to beam 4/0.5. This is most probably due to the effect of bond-slip between the concrete and steel reinforcement bars being neglected in the finite-element model. As the bond stresses for a given load in a beam with two reinforcement bars are higher than those in the beam with compared to one with four steel bars, hence, the effect of bond-slip is more prominent in the experimental result of beam 2/0.5. The analytical load–displacement curve for beam 2/0.5 is thus stiffer than those obtained experimentally. A closer approximation of the load–displacement behavior may be obtained if the effect of bond-slip is included in the simulation. Despite this, the analytical model is able to approximate the load–displacement curves up to 90% of the failure loads relatively well for the beams included in the present study.

Since the analytical model is stiffer than the actual beam, it is able to withstand a higher load for a given level of strain and, hence, displacement, compared to the actual beam. Thus, the analytical loads at failure are also slightly higher than the experimental results. The predicted loads at failure deviate 14.7% and 0.7% from the experimental failure loads for beams 2/0.5 and 4/0.5, respectively. A section of beam 4/0.5 failing in a shear mode and corresponding stress contour display along the load path is shown in Fig. 14. The locations where tensile cracks have formed have been outlined by the bold contour lines. This corresponds to the large shear cracks between the top and bottom load platens and along the mid-span of the actual failed specimen. This example illustrates the ability of the proposed failure surface to be incorporated into a constitutive model and applied in the analysis of concrete structures.

5. Conclusion

Biaxial experiments were conducted on plain concrete and SFRC plate specimens containing 0.5%, 1.0% and 1.5% of hooked fibers. The experimental results obtained were used to verify a failure surface proposed by Seow and Swaddiwudhipong [12]. The predictions of the failure surface fall within ±15% of the experimental stresses at failure and there is good agreement between the shapes of the theoretical and experimental biaxial failure curves. An equation to predict the strain at failure for SFRC under multi-axial loads, ε_{ci}, has also been proposed. These methods for predicting the stresses and strains at failure in SFRC under multi-axial loads were incorporated into a constitutive model. Finite-element analyses were carried out on SFRC plate and beam specimens to illustrate the application of these failure criteria. A good agreement is observed between the analytical and experimental results, thus validating the proposed failure surface and equation for predicting ε_{ci}.

References

[1] S. Swaddiwudhipong, H.R. Lu, T.H. Wee, Direct tension test and tensile strain capacity of concrete at early age, Cem. Concr. Res. 33 (12) (2003) 2077–2084.

[2] N.Z. Wang, S. Mindess, K. Ko, Fiber reinforced concrete beams under impact loading, Cem. Concr. Res. 26 (3) (1996) 363–376.

[3] H.D. Yan, W. Sun, H.S. Chen, The effect of silica fume and steel fiber on the dynamic mechanical performance of high-strength concrete, Cem. Concr. Res. 29 (3) (1999) 423–426.

[4] W.K. Yip, Generic form of stress–strain equations for concrete, Cem. Concr. Res. 28 (4) (1998) 499–508.

[5] S. Popovics, A numerical approach to the complete stress–strain curve of concrete, Cem. Concr. Res. 3 (5) (1973) 583–599.

[6] K.K. Tho, P.E.C. Seow, S. Swaddiwudhipong, Numerical method for analysis of concrete under multi-axial loads, Mag. Concr. Res. 55 (6) (2003) 537–547.

[7] D. Darwin, D.A. Pecknold, Nonlinear biaxial stress–strain law for concrete, ASCE, J. Eng. Mech. 103 (2) (1977) 229–241.

[8] D.P. Candappa, S. Setunge, J.G. Sanjayan, Stress versus strain relationship of high strength concrete under high lateral confinement, Cem. Concr. Res. 29 (12) (1999) 1977–1982.

[9] C.V. Nielsen, Triaxial behavior of high-strength concrete and mortar, ACI Mater. J. 95 (2) (1998) 144–151.

[10] X.D. Hu, R. Day, P. Dux, Biaxial failure model for fiber reinforced concrete, ASCE, J. Mater. Civ. Eng. 15 (6) (2003) 609–615.

[11] S.K. Padmarajaiah, A. Ramaswamy, A finite element assessment of flexural strength of prestressed concrete beams with fiber reinforcement, Cem. Concr. Comp. 24 (2) (2002) 229–241.

[12] P.E.C. Seow, S. Swaddiwudhipong, Failure surface for plain concrete and SFRC under multi-axial loads—a unified approach, ASCE, J. Mater. Civ. Eng. 17 (2) (2005) 219–228.

[13] T.Y. Lim, Elastic and post-cracking behavior of steel fiber concrete, Ph.D Thesis, The National University of Singapore, Singapore, 1987.

[14] British standards institution, BS 8110-1, Structural Use of Concrete—Part 1: Code of Practice for Design and Construction, BSI, London, 1997.

[15] P.E.C. Seow, A unified failure criterion for normal, high-strength and steel fiber-reinforced concrete, Ph.D Thesis, The National University of Singapore, Singapore, 2005.

[16] L.A. Traina, S.A. Mansour, Biaxial strength and deformational behavior of plain and steel fiber concrete, ACI Mater. J. 88 (4) (1991) 354–362.

[17] W.S. Yin, E.C.M. Su, M.A. Mansur, T.T.C. Hsu, Biaxial tests of plain and fiber concrete, ACI Mater. J. 86 (3) (1989) 236–243.

[18] J.C. Chern, H.J. Yang, H.W. Chen, Behavior of steel fiber reinforced concrete in multiaxial loading, ACI Mater. J. 89 (1) (1992) 32–40.

[19] P.E.C. Seow, S. Swaddiwudhipong, S.N.H. Mattar, Constitutive modeling of SFRC under multi-axial loads, Proc. the Sixteenth KKCNN Symposium on Civil Engineering, Korea, 2003, pp. 433–438.